

Accepted manuscript doi: 10.1680/jgein.22.00404

Accepted manuscript

As a service to our authors and readers, we are putting peer-reviewed accepted manuscripts (AM) online, in the Ahead of Print section of each journal web page, shortly after acceptance.

Disclaimer

The AM is yet to be copyedited and formatted in journal house style but can still be read and referenced by quoting its unique reference number, the digital object identifier (DOI). Once the AM has been typeset, an 'uncorrected proof' PDF will replace the 'accepted manuscript' PDF. These formatted articles may still be corrected by the authors. During the Production process, errors may be discovered which could affect the content, and all legal disclaimers that apply to the journal relate to these versions also.

Version of record

The final edited article will be published in PDF and HTML and will contain all author corrections and is considered the version of record. Authors wishing to reference an article published Ahead of Print should quote its DOI. When an issue becomes available, queuing Ahead of Print articles will move to that issue's Table of Contents. When the article is published in a journal issue, the full reference should be cited in addition to the DOI.

Accepted manuscript doi: 10.1680/jgein.22.00404

Submitted: 17 December 2022

Published online in ‘accepted manuscript’ format: 23 January 2023

Manuscript title: Effect of a soluble subgrade on leakage through a geomembrane defect

Authors: J. Fan and R. K. Rowe

Affiliation: Department of Civil Engineering, GeoEngineering Centre at Queen’s-RMC,
Queen’s University, Kingston, ON, Canada

Corresponding author: R. K. Rowe, Department of Civil Engineering, GeoEngineering
Centre at Queen’s-RMC, Queen’s University, Kingston, ON, Canada K7L 3N6.

E-mail: kerry.rowe@queensu.ca

Abstract

Leakage and erosion of a soluble subgrade overlain by a geomembrane with a 70-mm-long slit defect is examined. The subgrade (gypsum) solubility and its rate of dissolution from a solid state in contact with various solutions are investigated. In the absence of flow, the rate of dissolution is negligible. However, when there is flow there is dissolution, and if the flow is high enough, erosion. Erosion greatly increases fluid migration. The presence of an interface between the subgrade and a dissimilar material (e.g., a geomembrane) facilitates flow, dissolution, and erosion as the interface becomes an ever increasing preferential flow path, leading to a much greater leakage and erosion feature. The findings from this study highlight the risk of having a soluble subgrade below a single geomembrane used alone and exposed for the containment of liquids.

Keywords: Geosynthetics, Geomembrane, Reservoir, Gypsum, Interface flow, Erosion

1. Introduction

Geomembranes are widely used to contain fluids and protect the environment. Applications include modern municipal solid waste (MSW) landfills, leachate lagoons, stormwater attenuation ponds, sewage lagoons, storage ponds for process solutions, etc. (Giroud and Bonaparte 1989a, 1989b; Rowe 1998, 2005, 2012, 2020a; Rowe et al. 2004, 2013; Touze et al. 2008; Giroud 2016; Touze 2020; Rowe and Fan 2021, 2022; Fan and Rowe 2022a, 2022b, 2022c; Rowe and Jefferis 2022). In many cases, these systems may only involve a single geomembrane liner or a composite liner with a geomembrane over a geosynthetic clay liner or, if considered to be of sufficiently low permeability, the natural subgrade. With these geomembranes, the leakage (i.e., fluid flow under a hydraulic gradient) is effectively limited to flow through holes in the geomembrane (Giroud and Bonaparte 1989a, 1989b; Rowe 2012, 2020a; Abdelaal et al. 2014; Ewais et al. 2014; Rowe and Yu 2019; Gilson-Beck 2019). The magnitude of the leakage through a geomembrane hole is limited by the presence of a lower permeability material in contact with the geomembrane (e.g., Fukuoka 1986; Walton and Sagar 1990; Rowe 1998; Rowe and AbdelRazek 2019).

In the field, a significant fraction of observed leakage from geomembrane-lined reservoirs have been reported at or near the attachments between the geomembrane and a rigid structure (Giroud 2016). This may be caused by differential settlement between the soil beneath the geomembrane and the rigid structure, or repeated displacement arising from wind/wave action, or cycles of filling-emptying of the reservoir, etc. Seams are the weakest points of a geomembrane and therefore many of the problems (e.g., stress cracking) encountered in the field originate at seams welds (Peggs et al.

2005, 2014; Francey and Rowe 2022a,b; 2023). This is particularly true for extrusion welded seams at or near an attachment to a more rigid structure or penetration.

The subgrade soil beneath the liner is commonly what is available at the site with as little reworking as possible. Sometimes this is a gypsum rich soil. However, gypsum ($\text{CaSO}_4 \cdot 2\text{H}_2\text{O}$) is one of the most soluble and widespread minerals/soils (e.g., Australia; USA; China; UK, Europe especially Spain, Africa, and Middle East). The gypsum content varies widely from as low as less than 5% to as high as 50% (Kuttah and Sato 2015; Aldaood et al. 2014). Gypsum is frequently encountered in construction and civil engineering works due to the lack of economic alternative materials. For example, the gypsum-karst leakage problems have been reported to compromise the ability of dams, canals, and reservoirs to hold water. Even more seriously, gypsum rich soils have resulted in catastrophic failure and complete abandonment of the Upper Mangum Dam in Oklahoma, Quail Creek Dike in southwest Utah, Horsetooth and Carter Lake Dams in Colorado, and Anchor Dam in Wyoming (Johnson 2008).

This paper explores the implications of constructing a lined pond on a phosphogypsum subgrade (simply called gypsum throughout). Thus, the objectives of this paper are to: (1) estimate the solubility of gypsum in several different waters, (2) examine the rate of dissolution of compacted gypsum in contact with various solutions with the absence of advective flow; and (3) explore the flow path for leakage through a slit defect in an uncovered geomembrane (i.e., no ballast layer) with a hydraulic gradient.

2. Experimental Investigation

2.1 Test Material

The gypsum examined had similar physical properties like those reported by Rutherford et al. (1994). It was predominantly fine grained (~ 95% fines content) but with elevated levels of medium to fine-grained impurities and a hydraulic conductivity of about 3×10^{-7} m/s. The liquid limit of 23 was very close to its plastic limit of 22.

2.2 Solubility Test

The gypsum solubility was assessed in six solvents (Table 1). In Test 1, the solubility of gypsum was examined by progressively adding gypsum (solute) into the 1 L of solvent until the consequent increase in electrical conductivity of the solution was negligible and the added gypsum accumulated on the bottom of the beaker instead of dissolving. The electrical conductivity of the solution was measured after mixing the solution with an electric stirrer at 3 Hz for 24 hours after each addition of gypsum. A number of duplicate tests were conducted for Test 1 and the results were found to be repeatable (Table 1).

In Test 2, 8 g of gypsum was added to 1 L of solvent and the solution mixed until the electrical conductivity reached equilibrium. In both cases, the solubility limit of gypsum at room temperature was obtained by subtracting the mass of undissolved gypsum and impurities from the total mass added and dividing by the final volume of solution.

2.3 Dissolution Test

A dry mass of gypsum (1180 g) was compacted at a water content of 23% in a 1L graduated cylinder with a cross-sectional area of 3,040 mm² (62 mm in diameter). The initial average volume of gypsum in each column was 103 mL with a standard deviation of 1.8 mL. Once the plug was in place, 1L of test solution was very slowly introduced into the column, taking care to prevent any erosion of the gypsum surface. Two tests were conducted for each solution. In the first of each pair, the solution in the column was left undisturbed and simply monitored for conductivity (denoted the “no stirring test”). In the second test of each pair, the solution in the column was thoroughly mixed twice per day without disturbing the gypsum. The electrical conductivity of each solution was monitored each day. Once the electrical conductivity rose to a value corresponding to the half of the solubility limit, 500 mL of solution in the column was replaced by new solution and the process repeated.

2.4 Leakage and Erosion Test

The apparatus used for the leakage and erosion test was the same modified geosynthetic liner leakage simulator (GLLS) described by Rowe and Fan (2021, 2022). It comprised a rigid cylindrical steel test cell with an inside diameter of ~600 mm, and a height of 500 mm (see Fig. 1a). Two layers of geocomposite drains (GCDs) with a thickness of 15 mm were placed in the bottom of the cell. The 35-mm-thick coarse silica sand with particle sizes ranging from 2 mm (No. 6 sieve) to 3.35 mm (No. 10 sieve) was placed above the GCD. Gypsum, at 18% gravimetric water content, was compacted into the cell in three layers (Fig. 2a) until reaching a final thickness of 100 mm for each test. The as compacted dry density of the gypsum was approximately 1,600 kg/m³.

Two common scenarios were examined for a 2-mm-thick HDPE circular geomembrane with a 70-mm-long slit defect, cut by a sharp blade (Figs. 1, 2b, and 3), to simulate a knife cut, seam defect, or stress crack in a geomembrane. In the first scenario, the geomembrane with a slit was located over the gypsum near a simulated anchor trench (Figs. 1a, 1b, 1c). In the second scenario, the geomembrane with a slit was located over the gypsum near an attachment to a rigid structure (Fig. 1d). To prevent any preferential flow around the circumference of geomembrane, a bentonite perimeter seal was introduced around the top and bottom of the geomembrane edges except as explicitly indicated where Scenario 2 was being explored.

The anchor trench was simulated by a rectangular 2-mm-thick, 400 mm-long and 100 mm-wide HDPE panel (denoted GMB2) positioned vertically within the gypsum (Figs. 1a, 2a, and 2b). The vertical GMB2 was located 300 mm from the slit in GMB1 (Figs. 1b and 2b). A thin and shallow groove was cut in the surface of gypsum between the locations of the slit in GMB1 and the vertical GMB2 (Fig. 2b).

A total of four different GLLS tests were performed with different boundary conditions and the details of each specific set up presented in conjunction with the results in a later section.

3. Test Results

3.1 Solubility

There gypsum solubility was examined in six solvents (Table 1), namely:

- (i) Deionized water (initial electrical conductivity $< 2 \mu\text{S}/\text{cm}$), referred to as DI water. For the base case with pH ~ 6 , the gypsum solubility for Test 1 averaged 2.2 g/L and for Test 2 it was 2.6 g/L. Since the pH decreased by 1.1 units with the addition of the gypsum in Test 2, the effect of pH was examined by preparing two modified solvents by adding H_2SO_4 to DI water to shift the initial pH down to about 2.7 (denoted DI pH3) and 4.7 (DI pH5). In both cases the solubility was 2.4 g/L and 2.5 g/L for Tests 1 and 2, respectively. Based on the available data it would appear that the solubility of the gypsum tested averaged $2.4 \pm 0.15 \text{ g/L}$ (Standard deviation 0.15 g/L) in DI water with a final pH $\sim 5.0 \pm 1.1$.
- (ii) Kingston tap water with conductivity $\sim 303 \mu\text{S}/\text{cm}$, referred to as Tap water. To evaluate the effect of initial conductivity, the solubility was assessed in Kingston tap water to be about $2.2 \pm 0.12 \text{ g/L}$. Marginally lower than in DI water but at a higher final pH $\sim 7.8 \pm 0.3$.
- (iii) Salt water (a synthetic sea water) with a conductivity $\sim 43.3 \text{ mS}/\text{cm}$ ($43,300 \mu\text{S}/\text{cm}$) was prepared by adding 27.5 g/L sodium chloride to DI water. When added to this solvent, gypsum's solubility in salt water with pH =7.8 was 2.8 g/L.
- (iv) Natural sea water with conductivity $\sim 43.3 \text{ mS}/\text{cm}$ ($43,300 \mu\text{S}/\text{cm}$) was used as the final solvent. In this natural sea water with pH =7.9, the solubility of gypsum was highest at 3.1 g/L.

For all the solutions examined except the salt/sea water, the solubility limit of gypsum at room temperature averaged 2.4 ± 0.2 g/L, which is close to the 2.5 g/L solubility limit published by Moisset (1990) and 2.6 g/L by Van Alphen and Romero (1971). In the salt/sea water the gypsum had a slightly higher solubility of 2.8-3.1 g/L (Table 1). Thus, the solubility of gypsum in water appears to lie in the range 2.4-3.1 g/L, with the slightly higher solubility being for salt/sea water.

3.2 Dissolution

In the dissolution test, there was no flow through gypsum. This is to simulate the scenario where the only mechanism is dissolution of the gypsum in water. In the no stirring test, still water was in contact with gypsum in a static state. The stirring test was to simulate the potential disturbance induced by wind/wave action, or by cycles of filling-emptying of the reservoir.

The most effective means of monitoring the dissolution of gypsum was by periodically taking photographs to monitor the elevation at the surface of the compacted gypsum in each column.

Comparing the surface elevations of gypsum over a 52-day period, there was no discernable dissolution in any test with a maximum measurable possible decrease in the thickness of the gypsum being ≤ 0.1 mm (Fig. 4) or a rate < 0.0019 mm/day < 0.7 mm/year.

In summary, the test results show that in the absence of flow through gypsum, a soluble gypsum subgrade is very unlikely to be dissolved catastrophically.

3.3 Leakage and Erosion

Given that there was negligible dissolution of gypsum with no flow, a series of GLLS tests were designed to assess how a defect in the geomembrane and the potential flow paths affected leakage and erosion of gypsum for four cases with different boundary conditions beneath the gypsum (Fig. 5). For all the tests, water head overlying the geomembrane, denoted as H , began at 0.35 m for 24 hours (Fig. 6). It was subsequently increased to ~2 m where there was a slight decrease due to adjustment of flow through gypsum at this head along a preferential flow path that had begun to develop. H was progressively increased to ~6.3 m and stabilized thereafter until the termination of experiment after 14-15 days for Tests 1, 3, and 4. For Test 2, H stabilized at 1.6 m and the test was terminated after 6 days (Fig. 6). Leakage through the slit defect was collected through a tube connected to the bottom of the GLLS cell at the same elevation as the bottom of the GMB1 (Fig. 1a), and the volume was corrected to 20 °C based on the temperature of the collected leakage. The boundary condition beneath the gypsum and the subsequent test result for each GLLS test are presented in the following subsection. Tests 1 and 2 were to examine the effect of interface flow and subgrade conditions on leakage and piping. Test 3 and Test 4 were to examine the effect of vertical interface (simulated by vertical GMB and sidewall of GLLS), and a bad connection/defect between the geomembrane and a vertical structure on leakage, dissolution, and erosion.

3.3.1 Test 1

In Test 1, the gypsum was placed over a coarse silica sand layer to simulate a free draining boundary condition underlying the gypsum (Fig. 5a). Dividing the measured leakage Q by the corresponding water head H , the value of Q/H on Day 1 was initially small and around 2 L/d/m when $H = 0.35$ m. Increasing H to ~ 2 m, Q/H gradually rose from 6.5 to 23 L/d/m on Day 2, and then abruptly increased from 38 to 980 L/d/m on Day 3 with the inference of significant change in conditions below the geomembrane on Day 3. At the start of Day 4 the flow per unit head (Q/H) had reduced to about 400 L/d/m and slowly decreased with time to about 200 L/d/m at $H = 6.2$ m towards the end of the test.

After the test, exhumation of the geomembrane revealed a cavity eroded in the gypsum directly below the slit in GMB1 (Fig. 7). There was evidence of some water flow at the interface between the geomembrane and the gypsum in terms of very minor dissolution/erosion to the surface and the elimination of a groove placed to create a preferential path to the vertical GMB2 (Fig. 7a), there was no evidence of any dissolution or erosion at the anchor trench simulated by the vertical GMB2 or the rigid structure simulated by the sidewall of the GLLS cell. Rather, the flow took the path of least resistance to the drainage layer directly below the slit. Despite the excessive severity of the test in terms of the magnitude of the hydraulic gradient ($i > 62$) across the 100 mm thick gypsum (arising from the 6.2 m water head) and a consequent maximum flow rate of 1900 L/day in Test 1, the erosion cavity only extended to a depth of around 55 mm in the 100 mm thick gypsum layer (i.e., 45% of the thickness remained) after a 14 day-test. The deepest portion of the cavity was directly below the 70 mm slit in GMB1 (Fig. 7b). The shape of the cavity beneath the slit suggests a vortex was developed

likely due to water squirting through the slit and extended out in a quasi-circular manner to diameter of about 200 mm. In the description of results consider the top of the photograph in Fig. 7a as North. Although erosion was predominantly below the slit, there was also apparent backward erosion to the northeast and the total length of the erosion in that direction was about 280 mm, with the width of the offshoot to the northeast being about 80 mm and a depth of up to about 25 mm (Fig. 7b). The backward erosion is attributed to the surface irregularity and weaker zone on the surface of the gypsum. Given sufficient time and a substantially greater thickness of gypsum than 100 mm, there is a possibility of the backward erosion feature gradually extending towards the vertical GMB2 but not by the shortest route. This highlights the critical role played by minor heterogeneity in the gypsum that was present despite the consistent method of placement adopted. In this case flow was predominantly downward with only limited interfacial flow with the geomembrane and the gypsum being in a relatively good interface contact prior to cavity formation (Figure 8a).

The shape and volume (1.3 L) of the cavity was recorded with plaster cast (Fig. 7c) after a total 12,000 L seepage flow through the slit defect. Carefully exhuming the gypsum directly beneath the cavity revealed that the remaining gypsum remained in a compacted solid state and was not disturbed by the advective flow. Thus, the gypsum was removed in a dissolved state by advection. Given the volume of the cavity and the initial dry density of the gypsum, a total of approximately 1.6 kg gypsum was removed by 12,000 L seepage water. Thus, the average concentration required to remove the gypsum was 0.13 g/L which is well below the solubility limit of 2.4 g/L. The average depth of dissolution of gypsum below the geomembrane defect was 3.9 mm/day or 0.0045 mm/L of flow

through the hole. At this rate it would take 130 days to penetrate 0.5 m and about 110,000 L of flow.

Thus, this test shows that with active water flow through a defect in the geomembrane, gradual dissolution of the gypsum can occur even in the absence of any notable defect (e.g., interface or fracture) in the gypsum. Furthermore, a significant amount of time would be required to generate an extensive cavity even at the relatively high flow rate that occurred in this experiment.

3.3.2 Test 2

In Test 2, the coarse sand of Test 1 was replaced by pea gravel below a portion of gypsum in the area adjacent to the vertical GMB2 (Fig. 5b). The geotextiles in GCDs beneath the pea gravel were removed. Additionally, a 2-mm-thick HDPE GMB3 was placed above the silica sand and a portion of the pea gravel below the compacted gypsum below the slit to prevent downward Darcy flow from the slit to the sand. The absence of the geomembrane above most of the pea gravel created a drainage path from slit towards vertical GMB2 and downward to the pea gravel. This was to simulate the drainage that might be expected if there was some more permeable zone below the gypsum below the anchor trench than below the slit (i.e., variable drainage conditions below the gypsum; see Fig. 2c).

Similar to Test 1, Q/H on Day 1 for Test 2 was small and around 3.5 L/d/m when $H = 0.35$ m. Increasing H from 0.35 to 2 m, Q/H immediately increased to 3700 L/d/m and remained stable at ~3500 L/d/m from Day 2 until the end of test with $H = 1.6$ m. The effluent became turbid immediately after increasing H to 2 m (Fig. 9), showing that internal erosion occurred due to pea gravel below the gypsum at and near the anchor trench GMB2 (Figs. 2c, 5b and 10). The total flow over the 6 days of this test was 27000 L.

Exhumation of GMB1 and exposure of the gypsum revealed more severe erosion/dissolution in the six days of Test 2 (Fig. 10) than in the 14 days of Test 1 (Fig. 7). Similar to Test 1, there was evidence of vortex circulation flow beneath the slit giving rise to an essentially circular eroded depression about 250 mm in diameter (Fig. 10a). A schematic showing the inferred flow paths is depicted in Fig. 10b. Taking the top of photograph in Figs. 10a and 9b as North, the erosion progressed towards the east to the vertical GMB2 before eroding down the edge of GMB2 in both the north and south directions. Backward erosion developed to the north and then west away from the GMB2 (see the dashed line in the upward direction of Fig. 10b), with a local pathway of 17 mm-wide and opening out into a hole of 50 mm × 30 mm in dimension (Fig. 10a). Backward erosion also initiated in the east direction as water seeped away from the vertical GMB2 towards the sidewall of cell (Fig. 10b). Tests 1 and 2 both demonstrate backward erosion can occur in a weak zone in the gypsum adjacent to the flowing water and this can prompt an additional pathway.

The cavity below the slit in Test 2 eroded down 100 mm until it was stopped by GMB3 that acted as a barrier (Fig. 10d). There was no evidence of any flow through the cavity above GMB3 towards the drain and the water contained in the eroded bowl (cavity; Fig.10a) did not drain even though the test had been terminated 6 hours before taking this photograph. The interface flow along the vertical GMB2 gradually dissolved the gypsum as it flowed downwards to pea gravel near the center of GMB2 (Fig. 10c). Thus, in this case there was a gradual dissolution of the gypsum below the defect; but in the absence of a notable downward gradient below the defect, flow was predominantly at the interface between the geomembrane and the gypsum until the drainage conditions changed by

the combination of the presence of a downward interface at the simulated anchor trench combined with a highly permeable zone beneath the gypsum at this location (Figure 8b). Hence the relatively wide pathway from the slit to the simulated anchor trench indicated that the flow eroded the gypsum on the slit side as well as around the edges of GMB2 (Fig. 10b) and then down to the pea gravel on the far side of the slit (Fig. 10c). In the field, such an excessive dissolution at or near the attachment between geomembrane and rigid structure may exacerbate the pre-existing geomembrane defect and generate new defects, especially at a seam, due to differential settlement and the consequent tension within geomembrane (Giroud et al. 1995; Kavazanjian et al. 2017, Rowe and Yu 2019; Rowe and Shoaib 2017, 2018; Francey and Rowe 2022a,b, 2023).

3.3.3 Test 3

In Test 3, there was a circular GMB4 with a 75-mm-long and 50-mm-wide rectangular hole placed beneath the gypsum to simulate generally impermeable boundary (e.g., generally low permeability clay or intact rock) but with a local fracture zone beneath a small area of the simulated anchor trench. The local permeable zone was created by a rectangular hole in GMB4 and the small, unsealed gap between the circumference of GMB4 and cell side wall (acting as a nearby rigid structure) underlain by the same sand layer used in Test 1. In this case, the locally permeable zone below the gypsum and the boundary between GMB4 and sidewall acted as the potential preferential flow path (Figs. 5c and 5e).

On Day 1 ($H = 0.35$ m), Q/H was around 30 L/d/m. Subsequently, it increased to 170 L/d/m with the increasing H from 1.4 m to 4.8 m, followed by the decreasing Q/H to 30 L/d/m with a further increase in H to 6 m. Q/H oscillated with time with $Q/H = 40$ L/d/m ($H = 2.2$ m), 83 L/d/m ($H = 2.0$ m), 48 L/d/m ($H = 2.5$ m) between 0.96 and 1.85 days, 170 L/d/m ($H = 4.5$ m) on Day 4, 70 L/d/m ($H = 5.5$ m) on Day 5, 100 L/d/m ($H = 5.5$ m), and 130 L/d/m ($H = 6.4$ m) on Day 7. The oscillation of leakage indicated the potential internal erosion of gypsum occurred at some location due to hydraulic disturbing flow during the experiment, with the consequent collapse of old gypsum skeleton and the formation of a new equilibrium structure. Fan and Rowe (2022b) observed a similar phenomenon of leakage oscillation when investigating the ongoing piping of silty sand tailings through a circular geomembrane defect.

The total flow of 5,700 L in Test 3 was substantially less than that in previous tests and hence it is not surprising that exhumation of Test 3 revealed a substantially smaller cavity and hence dissolution of gypsum than in the previous two tests. However, there were several cavities/depressions on the surface of gypsum. One was 100 mm-diameter and 20 mm-deep beneath the slit (Figure 11a). There was also a cavity adjacent to the far side of the vertical GMB2, and four cavities at different locations at the sidewall of the GLLS (Figure 11a) that were notably deeper than that below the slit. Exhumation revealed that gypsum underneath the cavities at the interface with the GMB2 and the cell was highly disturbed and remarkably loose down to the edge of GMB4 or the rectangular hole beneath the GMB2. Apart from the distinct cavities, there was clear evidence that water had flowed around the edges of GMB2 causing dissolution of gypsum and exposure of GMB2 (originally flush

with the gypsum surface). In this case there was little evidence of erosion, the formation of the cavities appeared to be predominantly due to dissolution at locations of local weakness where flow was encouraged either by the presence of the slit or a more permeable pathway to the underlying sand. This test illustrated the significant role played by an advective pathway, with more discrete and remote pathways away from the slit than in Tests 1 and 2, there was a substantially less flow and dissolution despite the fact the test was run under a higher sustained head than in Test 1 for the same amount of time and a substantially shorter period of time than in Test 2.

3.3.4 Test 4

The boundary condition beneath the gypsum in Test 4 was identical to Test 3 except there was a bentonite perimeter seal around the edge of GMB4. This was to limit the drainage path to the rectangular hole in GMB4 (see Figs. 2d, 5d, and 5e).

On Day 1 with $H = 0.35$ m there was no flow, and the flow remained small at $Q/H = 5$ L/d/m on Day 2 when H was around 2 m. On Day 3 the flow increased from $Q/H = 6$ L/d/m to a peak value of 70 L/d/m when H was constant at 3 m. It then decreased to $Q/H = 3$ L/d/m with the increasing H from 4 m to 6 m, suggesting that the pathway had, at least partially, sealed up. Over the 15 days of this test the total flow was only 560 L.

In this case with a relatively small flow in the longest running test, there was only one shallow dissolution along the interface between gypsum and GMB2 eroding a small pathway around the southern portion of GMB2, exposing the GMB that had originally been flush with the surface of the gypsum and allowing the creation of a cavity on either side of GMB (Fig. 11b). Due to the low flow

rate (560 L over 15 days), there was no evidence of dissolution/erosion of the cavity directly underneath the slit. This verifies the observation that a noticeable dissolution of gypsum occurs with the presence of enough hydraulic disturbing energy to create a vortex below the slit. In the absence of a sufficiently high flow rate, the dissolution of gypsum below the slit was negligible. In this case the flow was predominantly interface flow until a preferential downward pathway was reached (Figure 8b).

4. Discussion

The transmissive zone between the geomembrane and the adjacent soil arises due to small irregularities at the interface (e.g., due to uneven subgrade and the rigidity of the geomembrane bridging small defects) between the two dissimilar materials that will allow fluid to migrate along the interface. Theoretical predictions and experimental evidences both prove that for a composite liner where the geomembrane is in direct contact with GCL/CCL, the interface transmissivity may be as important, and sometimes more important, than the hydraulic conductivity of the GCL/CCL in terms of controlling leakage through geomembrane defects (Giroud and Bonaparte 1989b, Rowe 1998, 2005, 2012, 2014, 2020b; Rowe and Abdelatty 2013; AbdelRazek and Rowe 2019; Rowe and AbdelRazek 2019; Rowe and Jabin 2021, 2022). Increasing the water head above the geomembrane liner on the one hand facilitated more flow through geomembrane defect due to a greater hydraulic gradient within the underlying subgrade; on the other hand, it imposed more pressure above the GMB1 and resulted in a better interface contact between GMB1 and the gypsum, decreasing the leakage rate. To some extent, the increased vertical pressure on the geomembrane near vertical GMB2

and the sidewall of GLLS cell can be expected to have increased horizontal pressure and reduce interface transmissivity at these two locations, both of which had the potential of reducing leakage.

With the increasing H , Q/H decreased after reaching the peak value for Tests 1, 3, and 4; while with a constant H of 1.6 m, Q/H remained constant in Test 2, the only case where significant erosion occurred. Therefore, owing to the interface flow, leakage through a geomembrane defect in water retention applications is not simply proportional to the overlying water head H as given by Darcy's Law, or proportional to $H^{0.5}$ as given by Bernoulli's equation.

Comparing the flow rate and erosion features (Figs. 7, 10, and 11), the extent of dissolution/erosion was directly correlated with the flow rate, with the severity of Test 2 ($Q= 27,000$ L/6 days = 4,500 L/d) > Test 1 ($Q= 12,000/14= 800$ L/d) > Test 3 ($Q= 5,700/14= 410$ L/d) > Test 4 ($Q= 560/15= 37$ L/d). The maximum leakage in Test 2 arose due to the interface flow along the gypsum and vertical GMB2 and filter incompatible free drainage boundary below GMB2.

For Test 1, given sufficient time and enough gypsum thickness, there is a great potential of developing a preferential interface flow path to the vertical GMB2 as the backward erosion feature gradually extending towards the GMB2.

With a generally impermeable boundary beneath the gypsum, leakage at a water head $H \sim 6$ m was 180 L/day for Test 3 and 20 L/day for Test 4, both of which were significantly smaller than 1,300 L/day for Test 1 ($H = 6$ m) and 5,600 L/day for Test 2 ($H = 1.6$ m) at the maximum head in the test. However, the notably greater electrical conductivity (Fig. 12) of the leakage at test termination for Test 3 (650 μ S/cm) and Test 4 (750 μ S/cm) than the tap water (303 μ S/cm) revealed that the

dissolution of gypsum was progressing at the lower flow rates of 180 L/day for Test 3 and 20 L/day for Test 4. Dissolution could be expected to continue and cavities in the gypsum would grow, eventually resulting in a greater leakage, which in turn can be expected to facilitate the propagation of erosion process when flow becomes sufficiently large (as was the case in Test 2).

For Test 3, the sudden increase and decrease in leakage and the gypsum paste found at the bottom of the GLLS cell suggest internal erosion may have been initiated followed by clogging of the interface between GMB4 and the sidewall of GLLS (Figs. 1a and 5e) down to the underlying coarse sand (Fig. 5c). Since the boundary between a soil and a rigid structure is likely to a measurable transmissivity and connections between a geomembrane and rigid structure are particularly prone to potential defects either initially or with stress cracking, this pathway is likely to significantly increase potential leakage, dissolution, and eventually erosion. The significance of this pathway is evident from a comparison of both the flow rates (180 L/day for Test 3 and 20 L/day for Test 4), the mass of gypsum removed (Figure 13), and the extent of cavity formation (Figures 11a and 11b).

In all tests there was a relatively low flow rate over the first day, and in some cases into the second day, providing the time needed for dissolution to be sufficient to notably raise the electrical conductivity of the effluent water (Fig. 12). As the flow rate increased the conductivity decreased, and during periods of particularly high flow the conductivity approached that of tap water that was being used as the permeant. This is considered to be because the short contact time between the water and the gypsum limited the amount of dissolution that could occur, although as is evident from the plot of cumulative mass dissolved versus time (Figure 13) that a larger flow even at a lower concentration

may result in larger mass removal. The largest mass removed was in Test 2 as may be expected due to the significant erosion that occurred despite the fact the test only ran for 6 days. The other 3 tests, which all ran for approximately 14 days, the conductivity reflected the variation in flow rate with time during the test and was most consistent for the longest time in Test 4 with the lowest flowrate, but since the flow was small the mass removed was also small (Figure 13).

5. Practical Implications

The results of this recent study demonstrated that a single geomembrane lined facility containing water and located on a gypsum rich subgrade is likely to experience problems if there is any flow through even a relatively small slit in the liner. In the absence of flow, the rate of dissolution of the gypsum may be very slow. However, as flow develops, the leakage will gradually dissolve and transport mass from below, and in the vicinity of, the hole. Depending on the gradient, the process can be quite slow based on the information provided from Test 1, with a 0.07 m long slit and a head of > 30 m, it would take more than 4 months to penetrate a 0.5 m-thick layer. Similarly, it might take 8 months to penetrate a 1 m thick layer with a head > 60 m, and even longer with a smaller head or a longer flow path. Thus, while it may take time, there is a considerable risk associated with a single geomembrane lined facility containing water on a gypsum rich subgrade.

The results also show that a defect in a geomembrane near a rigid boundary has a high potential of dissolution and ultimately erosion of the passageway at or near the interface. Thus, if there is a concrete dam on gypsum rich subgrade and the subgrade is lined with a single uncovered (i.e., no ballast layer) geomembrane in recognition of the potential for subgrade gypsum dissolution, there is

still considerable potential for problems to occur at geomembrane defects, especially one at or near the connection to the rigid structure. Thus, the potential failure modes and effects require very careful consideration if contemplating reliance on a single liner system over the gypsum rich subgrade.

6. Summary and Conclusions

Solubility tests and dissolution tests were conducted to examine the solubility limit of gypsum and the dissolution rate of compacted gypsum in contact with deionized water, tap water, sea water, and synthetic salt water, respectively. Leakage and erosion tests were conducted to quantify leakage and erosion process through a 70-mm-length slit geomembrane defect underlain by a soluble gypsum subgrade near an anchor trench or rigid appurtenant structure. For the specific conditions and materials examined, the following conclusions were reached:

1. The solubility limit of gypsum in deionized water, tap water, and sea water varied between 2-3 g/L. In the absence of flow through compacted gypsum, a soluble gypsum subgrade in direct contact with the aforementioned four solutions was extremely slow and less than 0.002 mm/day or less than 0.7 mm/year assuming the fluid was sufficiently mixed to ensure concentrations remain relatively low above the gypsum.
2. With intimate interface contact between geomembrane and underlying soil, fluid leaking through a 0.07 m long slit in the geomembrane caused dissolution of the gypsum at a rate of about 3.9 mm per day or 0.0045 mm per litre of flow to generate a 1.3 L cavity to a depth of 55 mm with about 12,000 L of flow in 14 days. Thus, the dissolution process is slow but persistent.

3. Significant backward dissolution occurred away from the defect due to the inferred presence of weaker zone on the surface of a nominally uniform gypsum layer. The dissolution extended 280 mm away from the hole within 14 days. Thus, given sufficient time, dissolution may occur in unpredictable locations extending under the geomembrane away from the originating defect. Pressure on the geomembrane from above has the potential to induce tensions in the vicinity of the cavity and ultimately inducing defects, particularly at and near the cavity.
4. For the soluble subgrade tested, an excessive dissolution and erosion feature was observed extending from the gypsum beneath the slit defect to a vertical structure and then down at the interface between the structure and the gypsum.

Acknowledgements

The research reported in this paper was supported by the Natural Sciences and Engineering Research Council of Canada (NSERC) under Strategic Grant STPGP 521237–18.

Data

Some or all data used are available from the corresponding author by request.

References

- Abdelaal, F. B., Rowe, R. K., and Brachman, R. W. I. (2014). Brittle rupture of an aged HPDE geomembrane at local gravel indentations under simulated field conditions. *Geosynthetics International*, 21(1), 1-23.
- AbdelRazek, A.Y. and Rowe, R.K. (2019) “Interface transmissivity of conventional and multi-component GCLs for three permeants”, *Geotext. Geomembr.*, 47(1):60-74

- Aldaoood, A., Bouasker, M., and Al-Mukhtar, M. (2014). Geotechnical properties of lime-treated gypseous soils. *Applied Clay Science*, 88, 39-48.
- Ewais, A. M. R., Rowe, R. K., Brachman, R. W. I., and Arnepalli, D. N. (2014). Service life of a high-density polyethylene geomembrane under simulated landfill conditions at 85 °C. *Journal of Geotechnical and Geoenvironmental Engineering*, 140(11), 04014060.
- Fan, J. Y., and Rowe, R. K. (2022a). Seepage through a circular geomembrane hole when covered by fine-grained tailings under filter incompatible conditions. *Canadian Geotechnical Journal*, 59(3), 410-423.
- Fan, J. Y., and Rowe, R. K. (2022b). Piping of silty sand tailings through a circular geomembrane hole. *Geotextiles and Geomembranes*, 50(1), 183-196.
- Fan, J. Y., and Rowe, R. K. (2022c). Effect of subgrade on tensile strains in a geomembrane for tailings storage applications. *Canadian Geotechnical Journal* (in press).
<https://doi.org/10.1139/cgj-2022-0019>
- Francey, W., and Rowe, R. K. (2022a). Stress Crack Resistance of unaged High-Density Polyethylene Geomembrane Fusion Seams. *Geosynthetics International*, 1-15.
<https://doi.org/10.1680/jgein.21.00027a> Published Online: 07April 2022
- Francey, W. and Rowe, R.K. (2022b) “Long-term Stress Crack Resistance of HDPE Fusion Seams Aged at 85°C in Synthetic Leachate” *Can. Geotech. J.*, (in press)

Francey, W. and Rowe, R.K. (2023) "Importance of thickness reduction and squeeze-out Std-OIT loss for HDPE geomembrane fusion seams", *Geotext. Geomembr.*, 51, 30-42;

<https://doi.org/10.1016/j.geotexmem.2022.09.003>

Fukuoka, M. 1986. Large scale permeability tests for geomembrane subgrade system. In Proceedings of the 3rd International conference on Geotextiles, Vienna, Austria, April 1986. Balkema Publications, Rotterdam, the Netherlands. Vol. 3, pp. 917–922.

Gilson-Beck, A. (2019). Controlling leakage through installed geomembranes using electrical leak location. *Geotextiles and Geomembranes*, 47(5), 697-710.

Giroud, J. P. (2016). Leakage control using geomembrane liners. *Soils and Rocks*, 39(3), 213-235.

Giroud, J. P., and Bonaparte, R. (1989a). Leakage through liners constructed with geomembranes—part I. Geomembrane liners. *Geotextiles and Geomembranes*, 8(1), 27-67.

Giroud, J. P., and Bonaparte, R. (1989b). Leakage through liners constructed with geomembranes—Part II. Composite liners. *Geotextiles and Geomembranes*, 8(2), 71-111.

Giroud, J. P., Bonaparte, R., Beech, J. F., and Gross, B. A. (1990). Design of soil layer-geosynthetic systems overlying voids. *Geotextiles and Geomembranes*, 9(1), 11-50.

Johnson, K. S. (2008). Gypsum-karst problems in constructing dams in the USA. *Environmental Geology*, 53(5), 945-950.

Kavazanjian, E., Andresen, J., and Gutierrez, A. (2017). "Experimental evaluation of HDPE geomembrane seam strain concentrations." *Geosynthetics International*, 24(4), 333-342.

Kuttah, D., and Sato, K. (2015). Review on the effect of gypsum content on soil behavior.

Transportation Geotechnics, 4, 28-37.

Moisset, J. (1990). Complete removal of radium from phosphogypsum. In *Proceedings of the Third*

International Symposium on Phosphogypsum, Orlando, FL, FIPR Pub (No. 01-060, p. 083).

Peggs, I. D., Gassner, F., Scheirs, J., Tan, D., Arango, A. M. N. and Burkard, B. (2014). Is there a

resurgence of stress cracking in HDPE geomembranes. *Proceedings 10th International*

Geosynthetics Conference, Berlin, Germany, DGGT, Essen, Germany (CD-ROM).

Peggs, I.D., Schmucker, B., and Carey, P. (2005). Assessment of maximum allowable strains in

polyethylene and polypropylene geomembranes. In *Proceedings of the Geo-Frontiers 2005*.

American Society of Civil Engineers, Reston, VA.

Rowe, R. K. (1998). Geosynthetics and the minimization of contaminant migration through barrier

systems beneath solid waste. In *Proceedings 6th International Conference on Geosynthetics*,

Atlanta 1, 27–103.

Rowe, R. K. (2005). Long-term performance of contaminant barrier systems. *Geotechnique*, 55(9),

631-678.

Rowe, R. K. (2012). Short and long-term leakage through composite liners. *Canadian Geotechnical*

Journal, 49(2), 141-169.

Rowe, R.K. (2014) “Performance of GCLs in liners for landfill and mining applications”, J. of

Environmental Geotechnics, 1(1): 3-21; <http://dx.doi.org/10.1680/envgeo.13.00031>

Rowe, R. K. (2020a). Protecting the Environment with Geosynthetics: 53rd Karl Terzaghi Lecture.

Journal of Geotechnical and Geoenvironmental Engineering, 146(9), 04020081.

Rowe, R.K. (2020b) “Geosynthetic clay liners: perceptions and misconceptions”, *Geotext.*

Geomembr., 48(2):137-156,

<https://doi.org/10.1016/j.geotexmem.2019.11.012>

Rowe, R. K., and Abdelatty, K. (2013). Leakage and contaminant transport through a single hole in

the geomembrane component of a composite liner. *Journal of Geotechnical and Geoenvironmental Engineering*, 139(3), 357-366.

Rowe, R. K., and AbdelRazek, A. Y. (2019). Effect of interface transmissivity and hydraulic

conductivity on contaminant migration through composite liners with wrinkles or failed seams.

Canadian Geotechnical Journal, 56(11), 1650-1667.

Rowe, R. K., and Fan, J. Y. (2021). Effect of geomembrane hole geometry on leakage overlain by

saturated tailings. *Geotextiles and Geomembranes*, 49(6), 1506-1518.

Rowe, R. K., and Fan, J. Y. (2022). A general solution for leakage through geomembrane defects

overlain by saturated tailings and underlain by highly permeable subgrade. *Geotextiles and*

Geomembranes, 50(4), 694-707.

Rowe, R.K. and Jabin, F. 2021. Effect of prehydration, permeant, and desiccation on

GCL/Geomembrane interface transmissivity. *Geotext. Geomembr.*, 49(6):1451-1469,

<https://doi.org/10.1016/j.geotexmem.2021.04.006>

Rowe, R.K. and Jabin, F. (2022) "Factors affecting Multicomponent GCL-Geomembrane Interface

Transmissivity for Landfills", *Geosynth. Int.*, Published Online: August 03, 2021.

<https://doi.org/10.1680/jgein.21.00042>

Rowe, R.K. and Jefferis, S. (2022). Protecting the environment from contamination with barrier

systems: advances and challenges, State-of-the-Art Lecture, Proceedings of the 20th International

Conference on Soil Mechanics and Geotechnical Engineering, Sydney, Australia, pp187-293.

Rowe, R. K., and Shoaib, M. (2017). "Long-term performance of high-density polyethylene (HDPE)

geomembrane seams in municipal solid waste (MSW) leachate." *Canadian Geotechnical Journal*,

54(12), 1623-1636.

Rowe, R. K., and Shoaib, M. (2018). "Durability of HDPE geomembrane seams immersed in brine for

three years." *Journal of Geotechnical and Geoenvironmental Engineering*, 144(2), 04017114.

Rowe, R. K., and Yu, Y. (2019). Magnitude and significance of tensile strains in geomembrane

landfill liners. *Geotextiles and Geomembranes*, 47(3), 439-458.

Rowe, R. K., Brachman, R. W. I., Irfan, H., Smith, M. E., and Thiel, R. (2013). Effect of underliner

on geomembrane strains in heap leach applications. *Geotextiles and Geomembranes*, 40, 37-47.

Rowe, R. K., Quigley, R. M., Brachman, R. W. I. and Booker, J. R. (2004). *Barrier systems for waste*

disposal facilities. London: Taylor & Francis (E & FN Spon).

Rutherford, P. M., Dudas, M. J., and Samek, R. A. (1994). Environmental impacts of

phosphogypsum. *Science of the total environment*, 149(1-2), 1-38.

Touze, N. (2020). Healing the world: a geosynthetics solution. *Geosynthetics International*, 1-31.

Touze, N., Lupo, J., and Barroso, M. (2008). Geoenvironmental applications of geosynthetics. *In*

Proceedings 4th European Geosynthetics Conference, Edinburgh, U.K.

Van Alphen, J.G., and Romero, F.D.R. (1971). Gypsiferous soils: notes on their characteristics and

management. Bulletin 12, International Institute for Land Reclamation and Improvement,

Wageningen, Netherlands.

Walton, J.C., and Sagar, B. (1990). Aspects of fluid flow through small flaws in membrane liners.

Environmental Science & Technology, 24, 920–924.

Table 1. Gypsum solubility tests

Solvent	Initial pH*	Final pH*	Mass of gypsum added (g)	Solubility ¹ Test 1 (g/L)	Solubility ^{1,3} Test 2 (g/L)
DI pH3	2.9, 2.6	4.1, 2.9	5.0, 8.0	2.4	2.5
DI Water	6.2, 6.0, 6.6	6.0, 5.7, 5.5	3.5, 5.3, 8.0	2.1, 2.3 ²	2.6
DI pH5	4.8, 4.5	5.7, 5.5	5.3, 8.0	2.4	2.5
Tap Water	7.1, 7.6, 7.0	8.0, 8.0, 7.4	3.6, 5.2, 8.0	2.1, 2.2 ²	2.4
Salt Water	8.4	7.8	8.0	-	2.8
Sea water	8	7.9	5.1	3.1	-

*pH measured before (initial) and after (final) all gypsum has been added.

¹Based on the mass of dry gypsum added to the solution minus that remaining in the bottom of the beaker when conductivity indicated there was negligible further solution of gypsum.

²“Duplicate” - Test 1

³Test 2 with 8g of gypsum added

Figure captions

Fig. 1. (a) Schematic of a typical GLLS (geosynthetic liner leakage simulator) cell used in leakage test; (b) Plan view of the slit (simulated stress crack) in GLLS test; (c) Simulated scenario 1: leakage through a defective seam close to the anchor trench; (d) Simulated scenario 2: leakage through a tensile rupture/defective seam next to attachment to a rigid structure

Fig. 2. GLLS test setup for (a) Preparation of gypsum; (b) Shallow groove from slit to vertical GMB 2 in the surface of compacted gypsum; (c) Configuration of coarse sand and pea gravel in Test 2; (d) Configuration of impermeable GMB 4 with bentonite perimeter seal around in Test 4.

Fig. 3. A 70-mm-length slit defect in GMB1

- Fig. 4. Photo of columns for the dissolution of gypsum specimens in direct contact with (a) DI water; (b) Kingston tap water; (c) Salt water; and (d) Sea water (Note: DI water represents Deionized water; Salt water is the synthetic water by adding sodium chloride into DI water until reaching the same conductivity as the Sea water)
- Fig. 5. Schematic of boundary configuration below gypsum in GLLS cell for (a) Coarse sand for Test 1; (b) Impermeable GMB3, pea gravel, coarse sand, geocomposite drain (GCD) with geotextiles removed beneath pea gravel for Test 2; (c) Impermeable GMB4 without bentonite perimeter seal around; (d) Impermeable GMB4 with bentonite perimeter seal around; and (e) Plan view of GMB4 with a rectangular hole beneath vertical GMB2
- Fig. 6. Water head H applied above the GMB in GLLS tests
- Fig. 7. Dissolution of gypsum in GLLS Test 1 for (a) Cavity in gypsum developed below the slit without fully penetrating 100-mm-thick gypsum after 14 days testing; (b) Some key dimensions of the cavity eroded in gypsum at test termination; (c) Plaster cast of cavity eroded in gypsum.
- Fig. 8. Schematic showing flow through GMB defect underlain by soluble subgrade for (a) Downward Darcy flow predominating; and (b) Interface flow predominating
- Fig. 9. (a) Turbid effluent collected between 1.03 and 1.04 days in Test 2; (b) Sediment after oven-drying demonstrating that it was gypsum that was eroded. Neither pea gravel nor coarse sand was found
- Fig. 10. Dissolution and erosion of gypsum in GLLS Test 2 for (a) Some key dimensions of the erosion at test termination; (b) Schematic representation of the inferred flow paths for water entering through the crack/slit and migrating to drain adjacent to the vertical geomembrane; (c) Cavities penetrating to the pea gravel on both the slit side and far side of the vertical GMB; (d) Cavity in gypsum below the slit penetrating to GMB3. (Note: water in the eroded bowl in Fig.10a had not drained in the 6 hours between termination the test and taking this photograph).
- Fig. 11. Photographs showing the surface of gypsum at test termination for (a) Test 3; (b) Test 4. (Note: dashed lines show contours of depression)
- Fig. 12. Conductivity of the collected leakage versus test duration in GLLS tests
- Fig. 13. The cumulative dissolution of gypsum in GLLS tests as water flow (calculated based on the conductivity of the leakage collected (Fig. 12) and the relationship between mass of gypsum dissolved per liter Kingston tap water and the conductivity of solution obtained when conducting the solubility test,

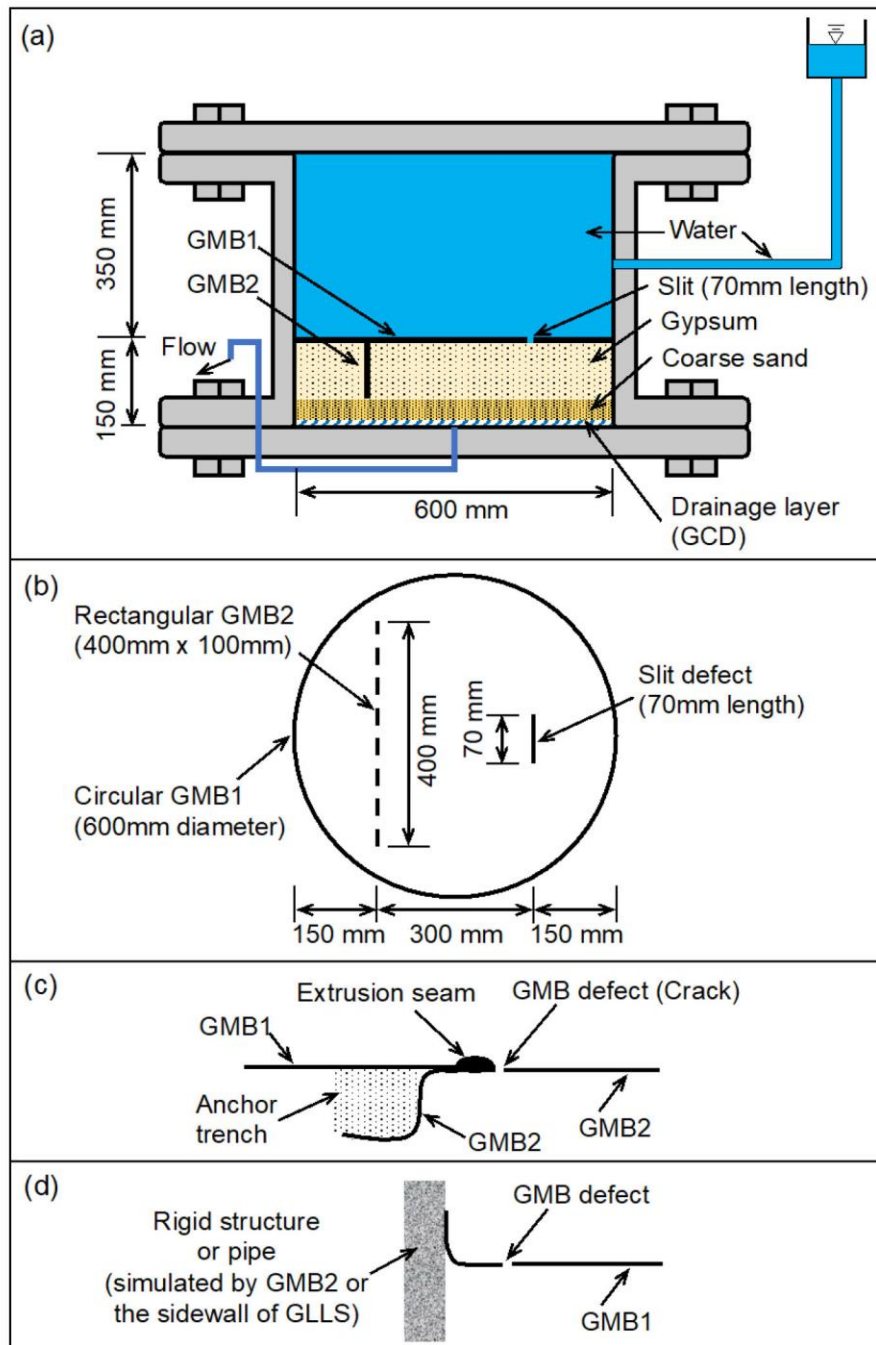


Figure 01

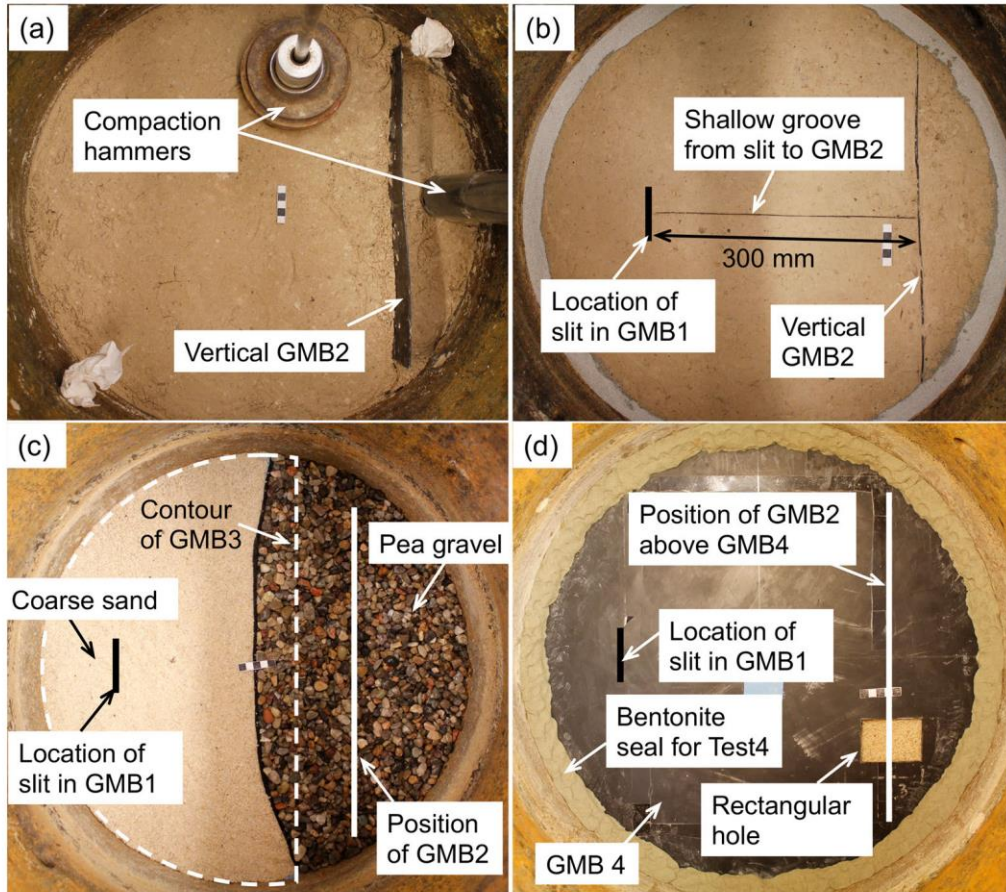


Figure 2

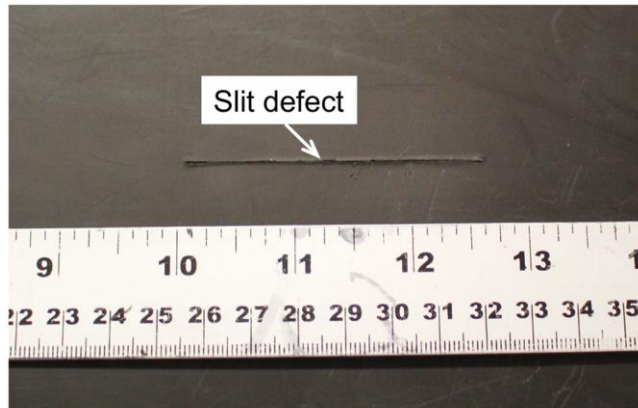


Figure 3

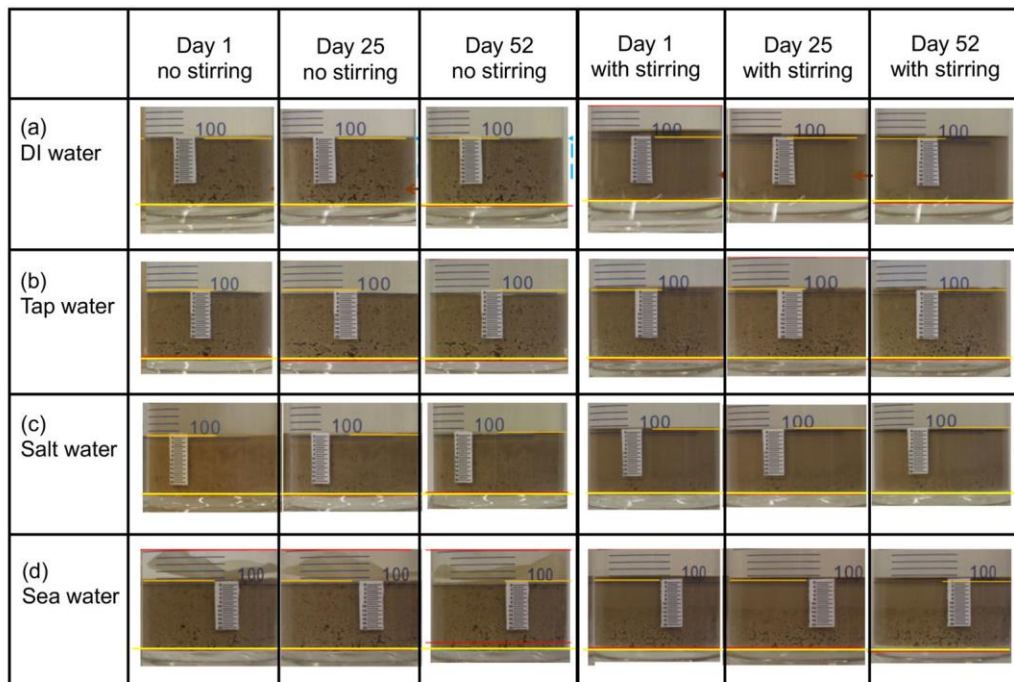


Figure 4

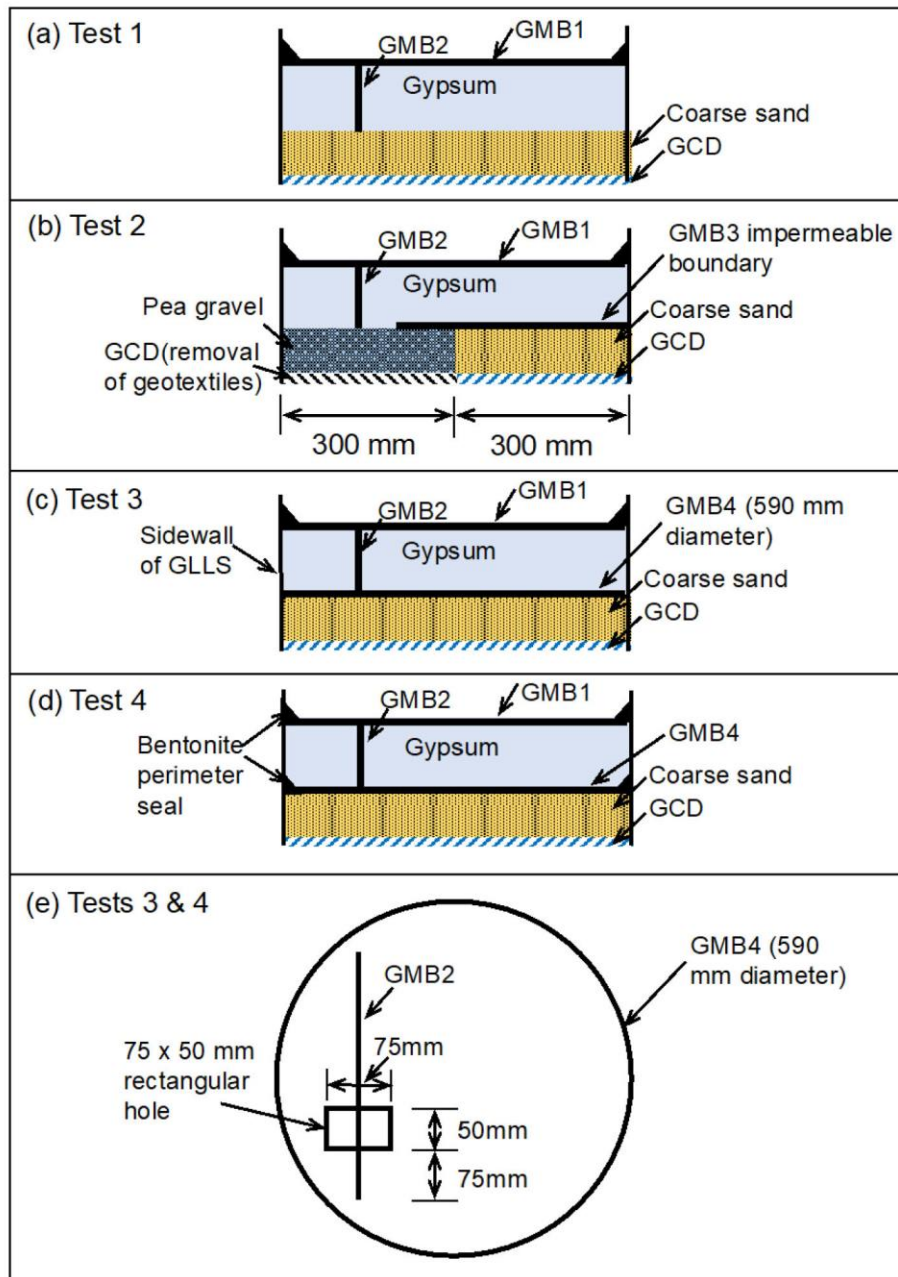


Figure 05

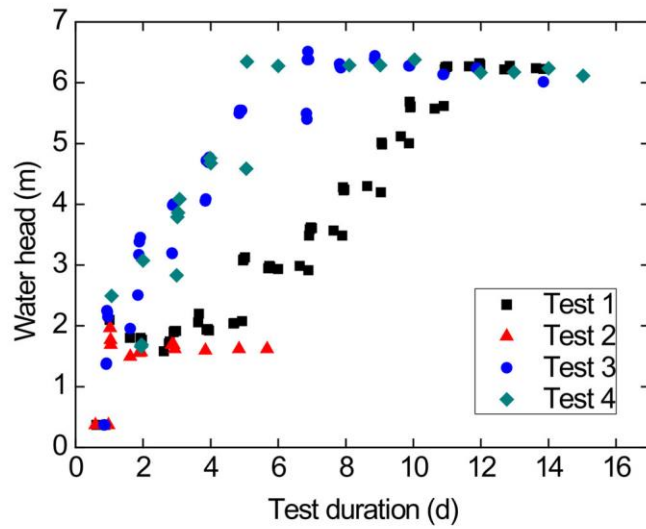


Figure 06

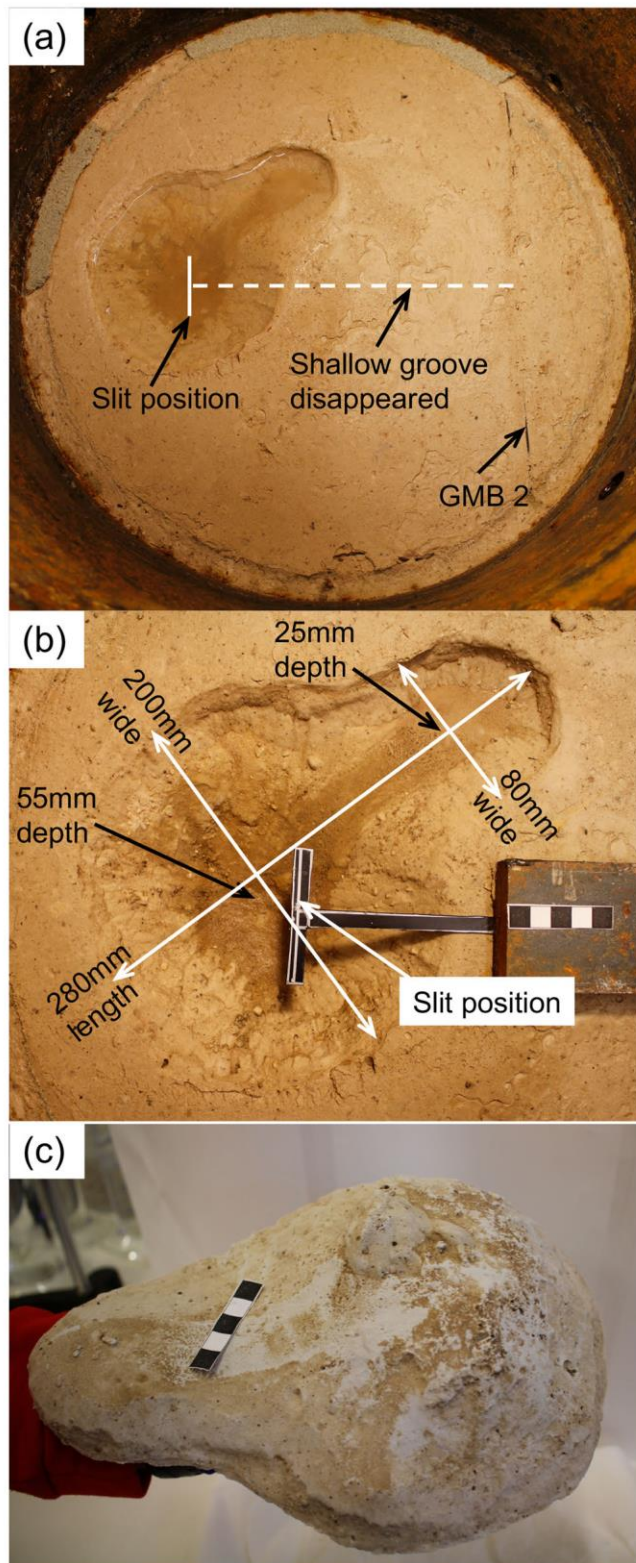


Figure 7

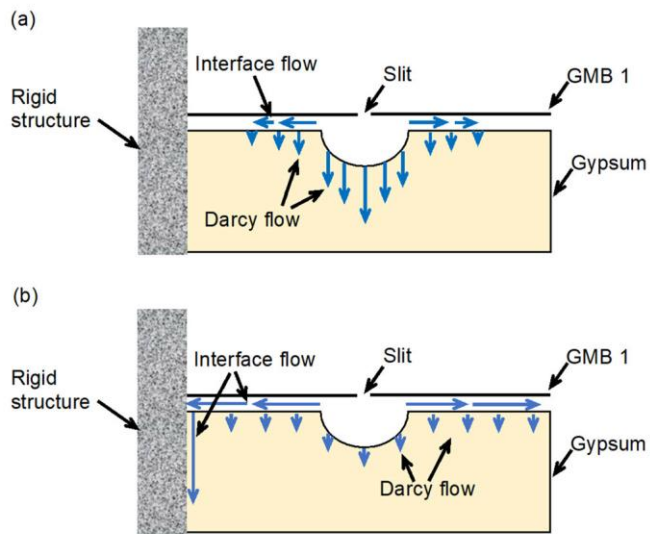


Figure 08

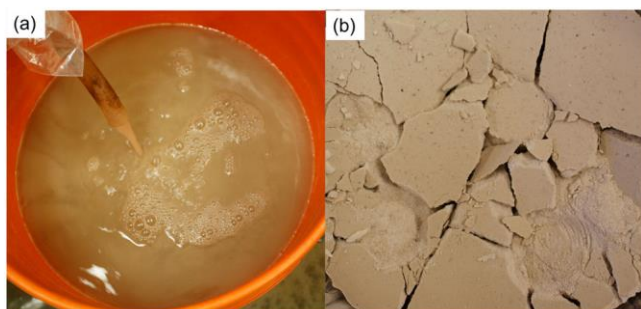


Figure 9

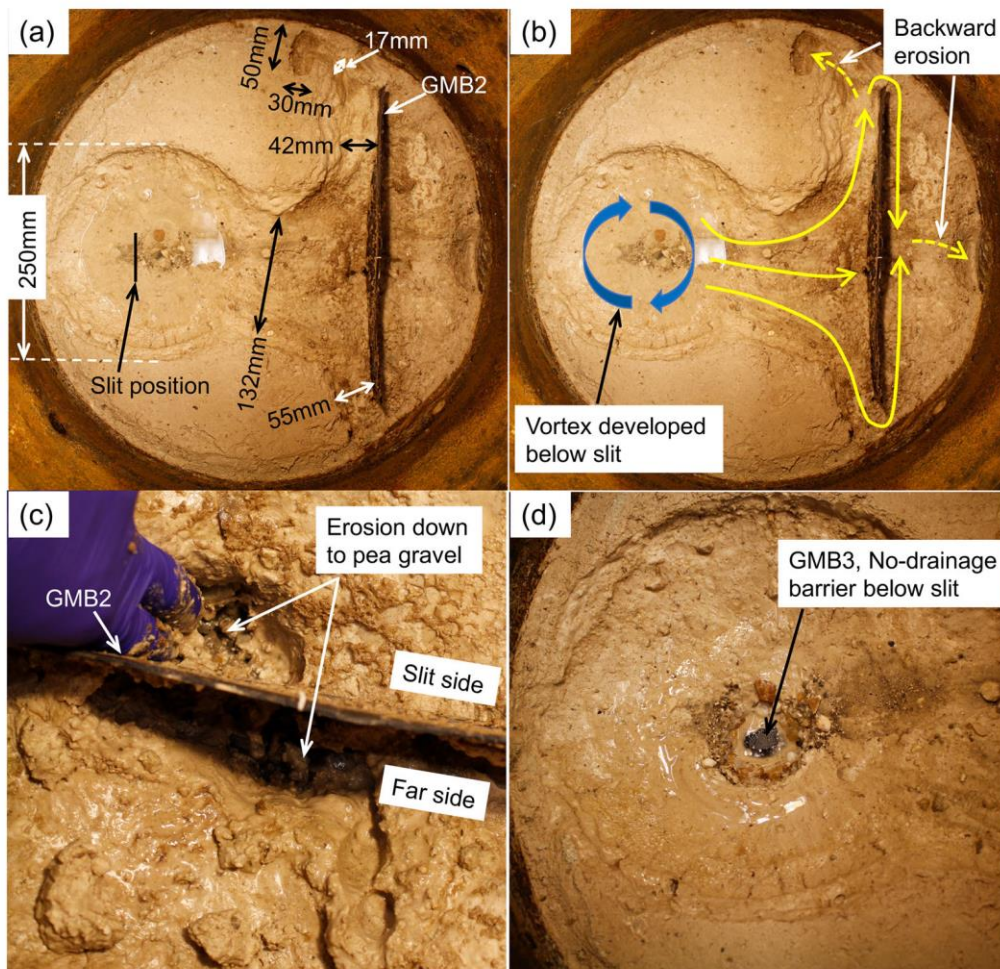


Figure 10

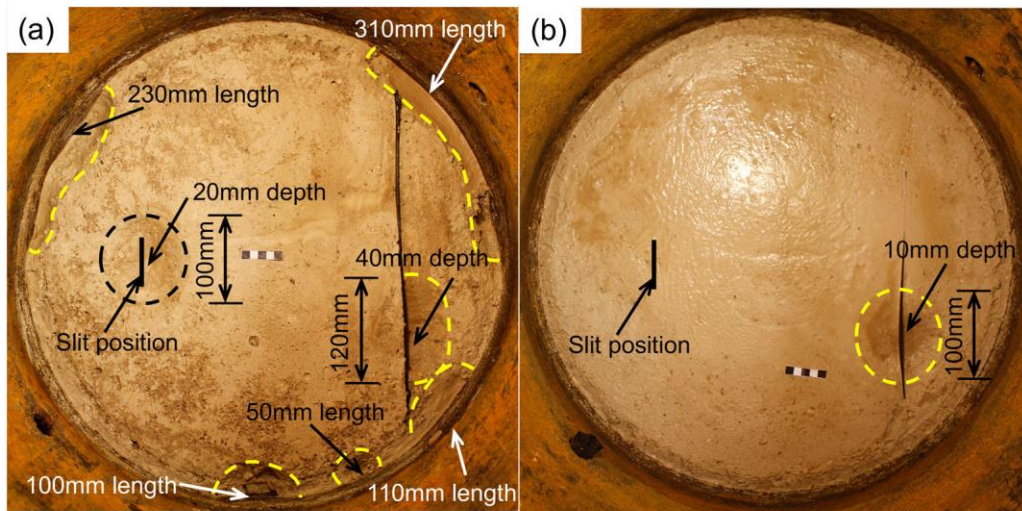


Figure 11

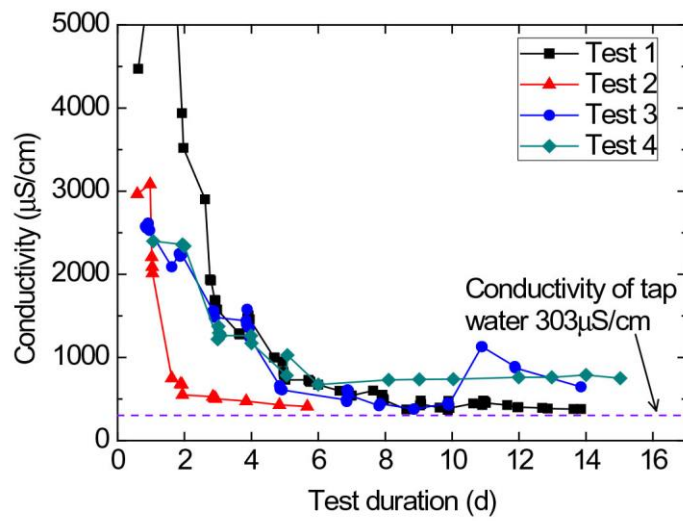


Figure 12

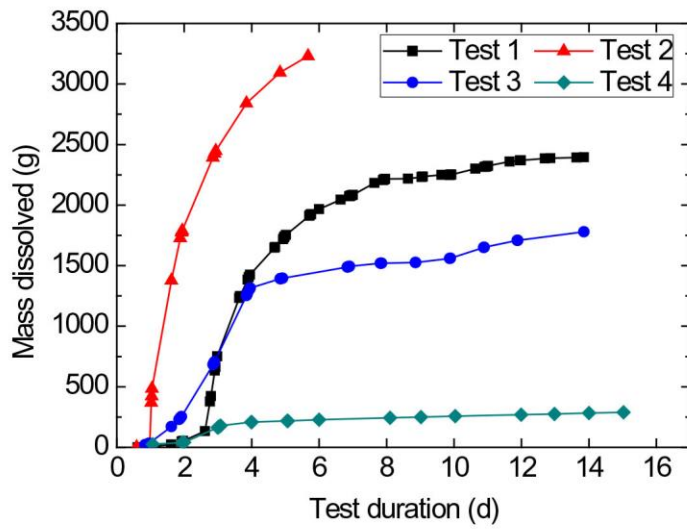


Figure 13